Effects of Pore Diffusion in the Catalytic Oxidation of Ethylene

L. S. CARETTO and KEN NOBE

University of California, Los Angeles, California

Effects of pore diffusion in the catalytic oxidation of ethylene on copper oxide-alumina have been studied by varying the catalyst size and maintaining constant the ratio of the tube to the pellet diameter. Hydrocarbon analysis was determined with a flame ionization detector; infrared analyzers were used to determine carbon monoxide and carbon dioxide concentrations. Other reaction products were analyzed with a gas chromatograph. Curvature of the Arrhenius plots and increase in reaction order with temperature indicated a transition region between kinetic control at lower temperatures and pore diffusion control at higher temperatures. A calculation procedure which was developed to predict the conversion considering pore diffusion effects provided satisfactorily agreement between calculated and experimental results.

The problems of pore diffusion in solid-catalyzed gaseous reactions have received much attention in recent years. The basic ideas are well treated in several texts (*5, 15, 18*). The usual approach is the calculation of an effectiveness factor, defined as the actual reaction rate divided by the rate which would be obtained if the entire catalyst surface had the same temperature and reactant concentration as the external surface. By calculating or estimating the effectiveness factor, one can judge whether or not pore diffusion effects are important. Unfortunately, a closed form solution for the effectiveness factor can be obtained in only a few cases, and except for isothermal first-order reactions, the effectiveness factor is dependent on the conditions at the external surface of an individual catalyst pellet. For most cases, then, the effectiveness factor varies between the entrance and exit of the catalyst bed.

Analyses of the pore diffusion problem readily show that the effectiveness factor is dependent on a characteristic dimension of the catalyst pellet. The experimental approach to determine pore diffusion effects, then, is to carry out the reaction under identical conditions with different sized catalyst pellets. If no difference in reaction rate is found, pore diffusion effects are not important.

We have previously published a calculation scheme for calculating the extent of a reaction when pore diffusion effects are important (*10*). In that paper some data for oxidation of cyclic C_6 hydrocarbons on copper oxide-alumina catalysts were used to test the calculation procedure, but all those data were obtained with a single pellet size. In addition, good agreement between experimental and calculated results was obtained only by postulating an unusually large effective diffusivity; it was pointed out that these effective diffusivities could be explained by possible surface diffusion.

It was desired to test this calculation procedure with data for a single reaction obtained from different pellet sizes. The reaction chosen was the catalytic oxidation of ethylene over copper oxide-alumina catalyst. This reaction was chosen because of previous work (*1, 13*) with ethylene oxidation on copper oxide catalysts and because if surface diffusion of hydrocarbons on the copper oxide-alumina were important, it should be less noticeable with ethylene, than with the C_6 compounds.

EXPERIMENTAL PROCEDURE

The experimental apparatus is shown in Figure 1. Air and ethylene were metered, introduced into a mixing chamber, passed through the catalyst bed, and exhausted to the atmosphere. Exit samples were continuously withdrawn from the reactor for analysis.

The laboratory air was first passed through a trap to remove traces of compressor oils and then through a bed of molecular sieve to remove water vapor and carbon dioxide. The molecular sieve was replaced every 6 to 10 hrs., depending on the flow rate. It was regenerated by passing a stream of air at 315°C. through the bed. The air flow rate was controlled with a pres-

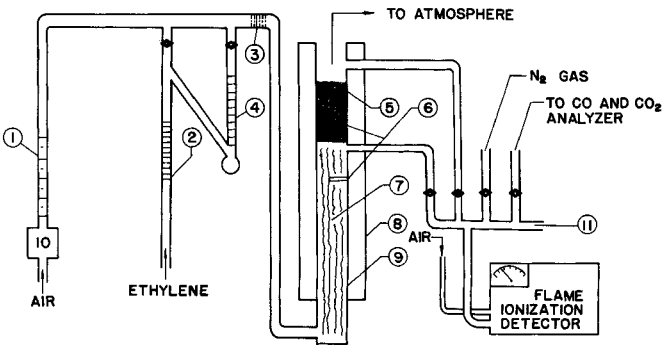

Fig. 1. Apparatus. 1 Main air flowmeter, 2 Ethylene flowmeter, 3 Mixing discs, 4 Soap bubble buret, 5 Catalyst bed, 6 Thermocouple wells, 7 Preheater, 8 Asbestos insulation, 9 Heating tapes, 10 Molecular sieve, 11 Sampling tube for chromatograph.

L. S. Caretto is at the University of California, Berkeley, California.

sure regulator and a Nupro precision needle valve and measured with a Fisher and Porter flowrator which had been previously calibrated with a wet test meter.

The ethylene (99.5% minimum purity) was used as received from the manufacturer. Its flow was also controlled with a pressure regulator and a precision needle valve. The ethylene normally passed through a small flowrator which was used for rough indicating purposes. Periodically, the ethylene flow was determined accurately by passing it through a soap bubble flowrator.

The mixing chamber and reactor tubes were constructed of pyrex. The reactor tubes were filled to a depth of approximately 50 cm. with pyrex distillation helices serving as an inert packing for the preheater section and as a base for the catalyst bed. No oxidation was observed for a reactor packed only with these helices at a temperature of 425°C., which was above temperatures attained in the experiments. Thus, the total amount of oxidation observed was due to the catalyst. Four different size reactor tubes were used in this study. Their inside diameters were 3.0, 2.2, 1.9, and 1.4 cm. The height of the catalyst bed was about two to two and one half times the diameter of the reactor tube. Each reactor tube had 1.5 mm. O. D. thermocouple wells mounted in the sides of the tube about 1.0 to 1.25 cm. apart. The wells were mounted at different angular positions in the tube to avoid setting up a preferential flow pattern.

The heat input was supplied by heating tapes wrapped around the reactor tube. The heating tapes were covered with asbestos. A 288 w. heating tape was used for the preheat section. The area surrounding the catalyst bed was wrapped with two to four (7/16 × 8 in.) 35 w. heating tapes. Each heating tape was controlled by a separate rheostat to minimize temperature gradients. The temperature profile was measured with iron-constantan thermocouples whose output was recorded on a Brown multipoint recorder.

The catalyst pellets were prepared in the manner previously described by Accomazzo (*1*). A batch of catalyst precipitate was prepared by mixing 120 g. wet Filtrol grade 90 alumina gel with a solution 91.2 g. of copper nitrate in 500 ml. of distilled water. After heating this mixture to 80°C. and stirring continuously, a solution of 42.4 g. of potassium hydroxide in 500 ml. of water was added as quickly as possible. The resulting mixture was heated and continuously stirred for 30 min. At the end of 30 min., a solution of 20 g. of potassium hydroxide in 500 ml. of distilled water was quickly added. The mixture was then left to cool at room temperature and the precipitate settled. The precipitate was washed several times until the wash solution was neutral. Four batches of wet precipitate prepared in this manner were thoroughly mixed together, pressed into molds, and heated in an oven at 150°C. for 8 hrs.

Four different pellet sizes were prepared. A summary of the physical properties of these pellets is given in Table 1. The B. E. T. surface area was determined by measuring the nitrogen adsorption isotherm. The pore volumes were determined by measuring the amount of water necessary to saturate a known weight of catalyst pellets. Although these measurements (pore volume and B. E. T. surface area) were made on the used catalysts, recent studies (*19*) have indicated that these properties remained essentially constant with use. In those studies, ethylene oxidation on the copper oxide-alumina pellets was continued for over 300 hr., with catalyst samples periodically withdrawn for pore volume and surface area determinations. The pore volume and surface area of the catalysts did not vary appreciably during the 300 hr. run.

Table 1. Physical Dimensions of Catalysts and Beds

Sample No.	1	2	3	4
diameter (cm.)	0.39	0.31	0.25	0.19
height	0.42	0.26	0.33	0.20
weight (g./pellet)	0.060	0.020	0.016	0.005
B.E.T. surface area (sq.m./g.)	93.7	89.6	90.6	96.3
pore volume (ml./gm.)	0.63	0.61	0.63	0.69
mean pore radius (Å.)	135.1	136.1	138.0	143.0
reactor tube diameter (cm.)	3.0	2.2	1.9	1.5
weight of catalyst bed (g.)	29.4	12.5	6.4	3.5
bed volume (ml.)	43.8	18.2	10.7	6.2

The catalyst was activated by passing air over the catalyst at a temperature of 480°C. for 48 hr. The air flow rate for activation was set to give a flow rate/catalyst weight of 80 liters/hr./g. of catalyst. The activation was followed by a 24 hr. breakin period, where conditions were set to give 90% oxidation (1,000 ppm., initial ethylene concentration) at the activation flow rate. A given catalyst bed was usually used for about 60 hr. The activity was periodically checked by repeating the initial run to ensure that the activity of the catalyst remained constant. The catalyst was analyzed for copper by an electroplating procedure. The percent of copper oxide in the catalyst was determined to be 48% by weight.

The standard hydrocarbon analyzer was a Beckman model 108 flame ionization detector. The analyzer was zeroed with air that had been passed over the catalyst at a temperature greater than 370°C. The initial concentrations of hydrocarbon were measured as the ratio of the volume flow rate of ethylene to the volume flow rate of air and were used to calibrate the analyzer. The flame ionization detector measured only hydrocarbons; it is not affected by carbon monoxide, carbon dioxide, or water.

Three different analyzers were used to check for the other reaction products. An infrared analyzer was used to check for carbon monoxide. It was calibrated by the manufacturer for 0 to 2,000 ppm. carbon monoxide and had a standard span gas which could be used to periodically standardize the analyzer. This analyzer was used only for spot checks, particularly, at the low conversion runs where the carbon monoxide would be likely to appear (if at all). The analyzer could measure a concentration of carbon monoxide as low as 5 ppm. Another infrared analyzer was used to measure the carbon dioxide concentration. This was calibrated in the laboratory for a 0 to 3,000 ppm. range. The calibration curve was checked periodically; little change was found, and the gain setting on the analyzer could be adjusted to keep one standard calibration curve. Again, this analyzer was used only for spot checks. The output from the hydrocarbon, carbon monoxide, and carbon dioxide analyzers were monitored on recorders.

The lines in the sampling system were fabricated from nylon or teflon. The sampling system was such that changes in the reactor could be detected by the flame ionizer in less than 10 sec. When changing from outlet to inlet readings, less than 15 sec. were required for the instrument to reach 95% of the inlet reading. The delay time for the infrared analyzers was about 30 sec.

A final check on other oxidation products was provided by a gas chromatograph with a thermal conductivity cell detector. The column was prepared by depositing 2-methyl-propene trimer on Johns-Manville C-22 firebrick. The column was packed in a 25 ft. length of copper tubing with an inside diameter of 0.19 in. The column was operated at room temperature with a helium carrier gas flow rate of 25 ml./min. Two milliliter samples which were taken from the reactor sampling manifold were injected into the column by means of hypodermic syringe. The column was able to separate air, carbon dioxide, ethylene, and ethylene oxide. It could not separate carbon monoxide from air. Under the given operating conditions the chromatograph was able to detect ethylene concentrations as low as 30 ppm.

In a given run the air flow rate was set, and the ethylene flow was adjusted to give the desired initial concentration. The sample system was then set to measure the outlet concentration, and no inlet readings were taken until steady state was achieved. After steady state conditions were achieved the outlet concentration was recorded and the sample system was set to measure the inlet concentration. After the inlet and outlet concentrations were recorded, the ethylene flow rate was measured accurately. The initial concentration was measured as the ratio of flow rates (ethylene/air). To make sure that the bypassed flow rate was the same as the flow rate for the normal flow path, the analyzer reading for the bypassed flow was compared to that of the normal flow. If they were different, the recorded initial concentration was corrected accordingly. The catalyst was always preheated to a high temperature (> 370°C.) before any measurements were taken. Although it was established that data taken by decreasing temperature were

the same as those taken by increasing temperature, a series of runs was usually started at the highest temperature and data were taken by decreasing the temperature. Usually 6 to 10 points were taken for a complete conversion-temperature curve.

The characteristics of the four different catalyst beds are given in Table 1. For each bed, four or five conversion-temperature curves were obtained. Care was taken to ensure that the bed remained a fixed bed under all conditions. In cases of imminent fluidization there were sharp fluctuations in the exit concentrations. Consistent data could not be obtained under these conditions.

RESULTS

The experimental variables ranged from 120 to 1,000 liters/hr. (NTP) in flow rate, 200 to 1,500 ppm in initial concentration of ethylene and 190 to 400°C. in temperature. Measured conversions ranged from 4 to 99%. The conversion decreased as initial concentration was increased, at constant flow rate and temperature. This indicates that the reaction order was less than one. The control of the temperature gradients in the bed represented a compromise between control of the axial and radial gradients. Since the axial gradients could be accounted for in the final calculations, it was considered more important to minimize the radial gradients. The largest observed differences from center line to wall were about 5°C. Typically, for axial temperature profiles, there was a sharp temperature rise just after the entrance to the bed, a maximum temperature and subsequent decrease towards the end of the bed, and in some cases, a small temperature rise near the end of the bed. The differences in center line temperatures (that is, $T_{max} - T_{min}$) increased as conversion increased. At conversions above 80% temperature, differences of 20°C. were typical. At intermediate conversions (30 to 60%) the maximum temperature difference was about 10°C.

Periodic checks on the reproducibility of the kinetic data showed no change in catalyst activity. This was expected since Accomazzo (*1*) had previously found that these catalysts showed no significant change in activity over a 1,000 hr. operating period. (His work involved oxidation of various hydrocarbons over a 140 to 540°C. temperature range.)

Measurements showed that there was no carbon monoxide present in the reactor products at any time. The carbon monoxide analyzer could detect as little as 5 ppm. carbon monoxide. Although it was only used for spot checks, it was always used on the low temperature runs. The carbon dioxide analyzer was able to detect within ± 40 ppm. Measurements of degree of oxidation by a carbon dioxide mass balance with the assumption of complete combustion provides a check on the ethylene

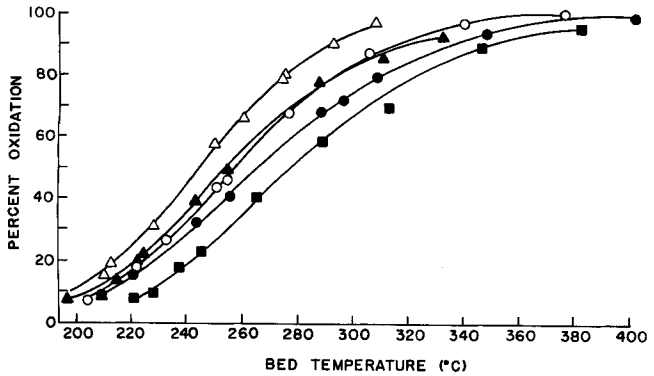

Fig. 2. Ethylene oxidation on sample 1. Initial concentration of ethylene in ppm. ▲ 200 at 1,000 liters/hr., ● 500 at 1,000 liters/hr., ■ 1,000 at 1,000 liters/hr., ○ 500 at 750 liters/hr., △ 500 at 500 liters/hr.

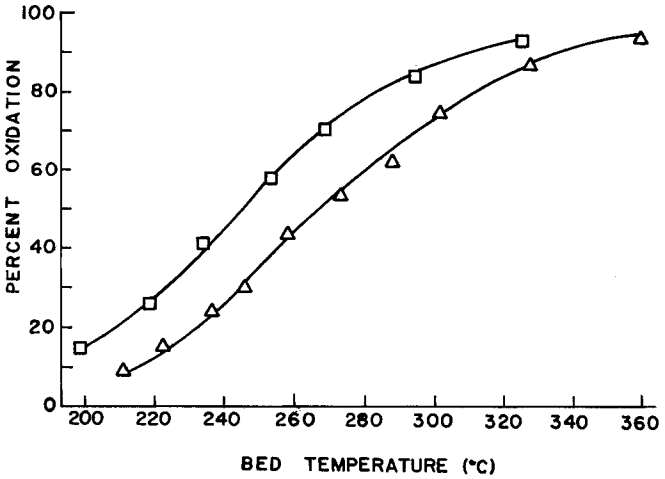

Fig. 3. Ethylene oxidation on sample 2 and 3. w/F = 7.0 × 10^6 g. catalyst — sec./mole. Initial concentration of ethylene = 200 ppm. △ Sample 2, □ Sample 3.

disappearance to within 20 ppm. The ethylene disappearance calculated from the flame ionization detector always agreed with that calculated from a carbon dioxide balance within this limit. Chromatographic analyses indicated no reaction products other than carbon dixoide.

Within the limits of the analyzers, the reaction was found to go to complete combustion, that is, to carbon dioxide and water. Therefore, for calculation purposes, it was assumed that the reaction was complete.

Some typical experimental data are plotted as conversion-temperature curves in Figures 2 to 5. Figures 3 to 5 each represent data taken at a common value of W/F and initial concentration. The differences in the curves represent data taken with different pellet sizes. In all these cases conversion at a given temperature is greater as the pellet size is decreased, indicating that pore diffusion is important in this reaction.

Rate Equation

Since the experimental data indicated that pore diffusion effects were important, only data at low temperatures, where the diffusion effects could be assumed negligible, were used to obtain a rate equation. Two simple Langmuir-Hinshelwood (Hougen-Watson) rate models were tried but rejected since they gave a poor correlation of the data and the coefficients obtained were physically meaningless. It was found, however, that the data were well correlated by the simple power law rate expression

$$r = k_p P^n \quad \text{where} \quad k_p = Ae^{-E/RT} \qquad (1)$$

Although there has been much discussion in the recent literature about the efficacy (*12*) of various rate equa-

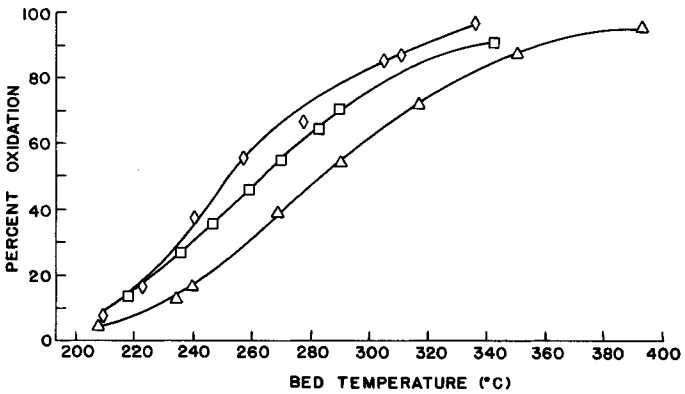

Fig. 4. Effect of pellet size on ethylene oxidation. w/F = 2.8 × 10^6 g. catalyst — sec./mole. Initial concentration of ethylene = 500 ppm. △ Sample 2, □ Sample 3, ◇ Sample 4.

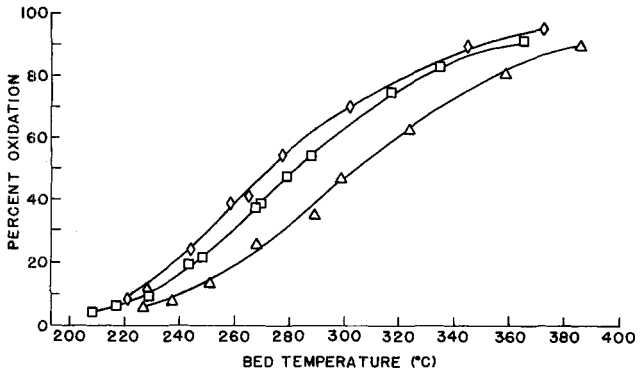

Fig. 5. Effect of pellet size on ethylene oxidation. w/F = 1.4 × 10^6 g. catalyst — sec./mole. Initial concentration of ethylene = 1,000 ppm. △ Sample 2, □ Sample 3, ◇ Sample 4.

tions, it is generally considered that the simple rate equation is adequate if it provides good representation of the data. The actual reaction path is undoubtedly very complicated in this reaction and any sophisticated rate equation used would be no more than an empirical representation of the data obtained.

The observed reaction order with the low temperature data was 1/5. The applicability of this rate equation and reaction order over the complete range of experimental conditions was then verified in two ways. First, the simple analysis was applied to the high temperature data to obtain an apparent reaction order. It was found that the apparent reaction order increased with temperature reaching a value of 0.6 at higher temperatures. This observation confirmed the validity of the 1/5 reaction order since it is wellknown (*18*) that *n*th-order reactions exhibit an apparent reaction order of $(n + 1)/2$ in regions of pore diffusion control. To further verify the rate model chosen, the apparent kinetic rate constants at high temperatures were calculated and plotted in the usual Arrhenius plot (Figure 6). It was found that the apparent activation energy decreased as temperature increased. This provides further evidence (*18*) that the data were taken in a transition region between kinetic control and pore diffusion control. Based on all this evidence the power law rate equation with $n = 1/5$ was used for further calculations.

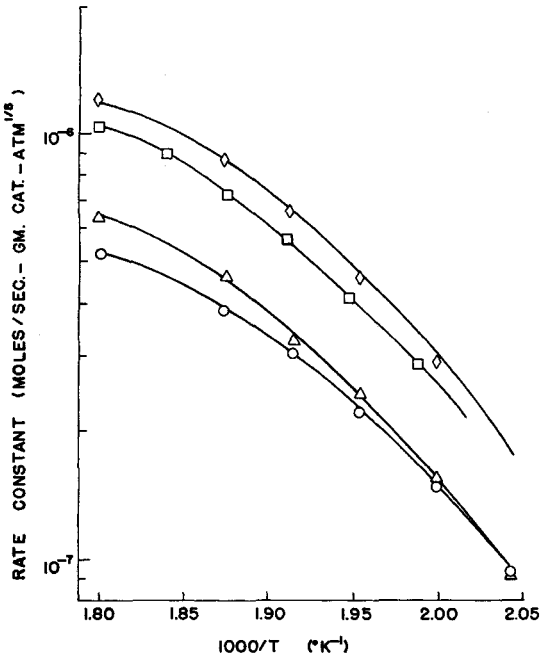

Fig. 6. Arrhenius plot of catalytic ethylene oxidation. ○ Sample 1, △ Sample 2, □ Sample 3 ◇ Sample 4.

PORE DIFFUSION CALCULATIONS

The differential equations governing pore diffusion are readily derived by taking an energy balance and a mass balance on the reaction component and writing the transport processes as pure conduction and pure diffusion. This defines an effective diffusivity and an effective thermal conductivity. The important considerations associated with solution of these equations are pellet geometry, reaction rate expression, evaluation of effective transport properties and coupling between temperature rise due to heat of reaction and reaction rate.

Exact solutions are available for isothermal first-order reactions in various pellet shapes (*3*). Aris has shown that for finite cylinders the effectiveness factor for the isothermal first-order case is

$$\eta = 1 - \frac{32}{\pi^2} \sum_{m=1}^{\infty} \sum_{n=0}^{\infty} \frac{1}{(2n+1)^2 j_m^2} \cdot \frac{\lambda^2 a^2}{\lambda^2 a^2 + j_m^2 + (2n+1)^2 \pi^2 a^2 / l^2} \quad (2)$$

where λa is the diffusion modulus $a\sqrt{k_v/D_e}$.

Aris (*4*) and Bischoff (*6*) showed that the usual diffusion modulus for flat plates could be normalized so that the curves of effectiveness factor of the normalized modulus were the same for all rate expressions in the strong diffusion region. This normalized modulus was given by

$$\lambda_n L = \frac{L\, r_v(C_x)}{\left\{ 2 \int_o^{C_x} D_e(C) r_v(C) dC \right\}^{1/2}} \quad (3)$$

Bischoff showed further that the curves of effectiveness factor vs. the normalized modulus also matched in the low diffusion region and that the differences which occurred in the intermediate region were small. (For a given value of the normalized modulus, exact values of effectiveness factor calculated for different reaction orders between 0 and 3 differed by no more than about 30%.) Thus, if one uses the normalized modulus, one can obtain a good approximation of the effectiveness factor for an n^{th}-order reaction over the entire region (exact for weak and strong diffusion regions) by using the effectiveness factor vs. normalized modulus relation for any reaction order.

Numerical solutions of effectiveness factor for a 1/5 order rate equation have been obtained (*9*). These values can be used to obtain the relation between effectiveness factor and normalized modulus for the 1/5 order. When this is done, it can be shown that the maximum error due to using the effectiveness factor equation for first-order rate equations to calculate the effectiveness factor for 1/5 order is less than 13%. Although the normalized modulus concept was derived for the flat plate, the characteristic length can be divided out of both sides of Equation (3) and one can obtain an expression for the modulus, λ_n, which depends only on the concentration and not on physical dimensions. In particular, for D_e constant and $r_v = k_v C^n$, Equation (3) becomes

$$\lambda_n = \frac{k_v C_x^n}{\left\{ 2 D_e k_v \int_o^{C_x} C^n dC \right\}^{1/2}} = \sqrt{\frac{k_v C_x^{n-1}}{D_e} \frac{n+1}{2}} \quad (4)$$

If this λ_n is used in place of λ, Equation (2) may then be used to calculate the effectiveness factor for n^{th} order reactions.

The effective diffusivity represents the diffusion coefficient for the reactant in the catalyst pellet at reaction conditions. Since it is usually not possible to measure a

pure diffusion process under these conditions, the evaluation of the effective diffusivity is usually split into two problems. The first is the evaluation of the homogeneous gas phase diffusion coefficient for the reactant in a cylindrical channel with a radius equal to the mean pore radius of the pellet. The second is the establishment of the diffusivity ratio. The former question often involves diffusion conditions which are intermediate between those of ordinary bulk gas phase diffusion and Knudsen diffusion. In this region the average diffusion coefficient is well represented by the Bonsanquet interpolation formula (*7, 16*).

$$\frac{1}{D} = \frac{1}{D_k} + \frac{1}{D_{ab}} \tag{5}$$

The diffusivity ratio can be determined experimentally for a pair of test gases or estimated by various empirical formulae. The Weisz-Schwartz (*20*) formula

$$\frac{D_e}{D} = \frac{\epsilon^2}{\sqrt{3}} \tag{6}$$

has been shown to give good agreement between calculated and measured values of the diffusivity ratio and is used here. It should be noted that the diffusivity ratio is thus calculated *a priori* from porosity data and is not an adjustable factor. From Equations (5) and (6), the effective diffusivity is given by

$$D_e^{-1} = \frac{\sqrt{3}}{\epsilon^2}\left(D_k^{-1} + D_{ab}^{-1}\right) \tag{7}$$

Although this is actually a multicomponent diffusion problem, the ethylene concentrations (and consequently product concentrations) were so low that the ordinary diffusion coefficient could be taken as the binary ethylene-air diffusion coefficient.

A general analytical expression for the effectiveness factor cannot be obtained if it is necessary to take heat effects into account. If the assumption of an isothermal pellet is valid, the above development can be used to evaluate the effectiveness factor. The relation between temperature and concentration is given by the formula of Damköhler (*11*) which has been shown to apply to all pellet shapes by Prater (*17*).

$$\left(\frac{T}{T_x} - 1\right) = \beta\left(1 - \frac{C}{C_x}\right) \tag{8}$$

where

$$\beta = \frac{(-\Delta H_R) D_e C_x}{T_x \kappa_e} \tag{9}$$

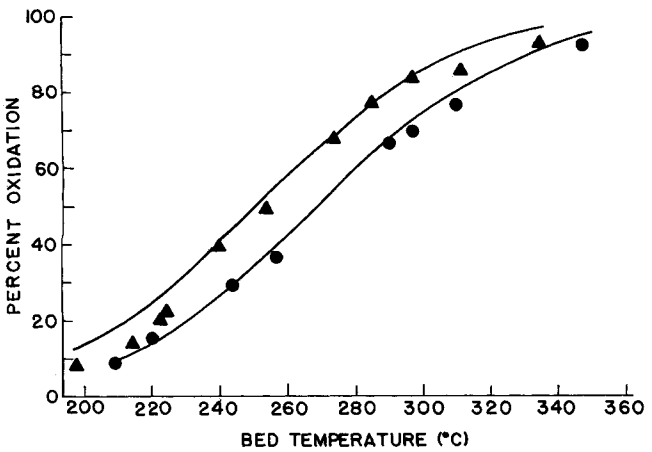

Fig. 7. Calculated and experimental data of ethylene oxidation on sample 1. Initial concentration of ethylene in ppm. ▲ 200 at 1,000 liters/hr., ● 500 at 1,000 liters/hr. Lines: calculated data. Points: experimental data.

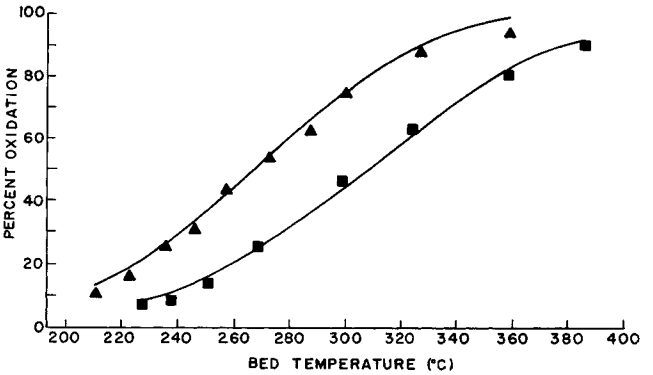

Fig. 8. Calculated and experimental data of ethylene oxidation on sample 2. Initial concentration of ethylene in ppm. ▲ 200 at 780 liters/hr., ● 1,000 at 780 liters/hr. Lines: calculated data. Points: experimental data.

Temperature effects in pore diffusion are described by two parameters, β, defined above, and γ, where

$$\gamma = \frac{E}{RT_x} \tag{10}$$

In cases where the temperature gradients are small compared to the external surface temperature, a single parameter equal to the product $\beta\gamma$ is sufficient to calculate thermal effects (*8*). For small temperature gradients in spherical pellets, Anderson (*2*) has derived an equation for the discrepancy between the observed rate constant and the rate constant evaluated at the temperature of the external surface, in terms of observable quantities.

$$\frac{\bar{k}_v - k_v(T_x)}{k_v(T_x)} = \frac{-\Delta H_R \bar{r}_v \rho^2 E}{15\ RT_x^2 \kappa_e} \tag{11}$$

Using Equations (4), (9), and (10) and writing $\bar{r}_v = k_v(T_x) C_x^n$ one obtains

$$\frac{\bar{k}_v - k_v(T_x)}{k_v(T_x)} = \frac{\beta\gamma\eta\lambda_n^2\rho^2}{15\left(\frac{n+1}{2}\right)} \tag{12}$$

If the heat effects parameter, $\beta\gamma$, is small, the following equation for the effectiveness factor of an n^{th} order reaction in the strong diffusion region can be obtained (see Appendix).

$$\eta = \frac{3}{\lambda_n \rho}\left(1 + \frac{\beta\gamma}{n+2}\right)^{1/2} \tag{13}$$

Substituting this into Equation (12) gives

$$\frac{\bar{k}_v - k_v(T_x)}{k_v(T_x)} = \frac{\beta\gamma\lambda_n\rho}{5\left(\frac{n+1}{2}\right)}\left(1 + \frac{\beta\gamma}{n+2}\right)^{1/2} \tag{14}$$

In the worst case the discrepancy in the rate constant caused by assuming an isothermal pellet was less than 4%. Details of this calculation are given in (*9*). In the following calculations, then, an isothermal pellet will be assumed.*

In calculating the exit conversions, plug flow is assumed and radial temperature gradients are neglected. The usual design equation for catalytic flow reactors is written in finite difference form

* The maximum temperature difference, as calculated from Equation (8) by assuming C = 0, was less than 0.3°C. However, even this small difference in temperature can cause the 4% discrepancy in rate constant.

$$\frac{\Delta w}{F} = \frac{\Delta x}{r_{avg}} \qquad (15)$$

and the conversion across each increment of catalyst weight is calculated. In order to account for the nonisothermal bed, the temperature at the end of each increment must be known. In these calculations the measured temperature profile was plotted and temperatures at the end of the increments were determined from the graphs. An outline of the calculation procedure for a given increment follows:

1. Estimate a value of the rate at the end of the increment.
2. From this the average rate and then the conversion across the increment are determined. From the conversion the bulk concentration of the reactant is determined.
3. The heat and mass transfer correlations of Yoshida, Ramaswami, and Hougen (*21*) are used to calculate the temperature and partial pressure difference between the bulk stream and the external surface of the catalyst.
4. The rate is calculated as $\eta(T_x, C_x)k_v(T_x)C_x^n$.
5. A trial and error calculation is made until the reaction rate and heat and mass transfer rates are satisfactorily consistent.
6. The value of the rate calculated is compared to the guessed value and another trial and error calculation is made until two subsequent calculations of the rate agree within a prespecified tolerance.

The detailed equations (except for the use of the normalized modulus and accounting for heat transfer between the bulk gas stream and external catalyst surface) have been given previously (*10*).

The values of A and E initially used in the rate expression were estimated by assuming negligible diffusion effects in the low temperature data on the smallest pellet sizes. These values did not give satisfactory agreement between experimental and calculated conversions and were adjusted until such agreement was obtained. The final rate expression used was

$$r = 125.5\ e^{-19{,}500/RT}\ P^{1/5} \qquad (16)$$

Comparison of experimental and calculated results is shown in Figures 7 to 10. Here the lines are calculated results while the plotted points represents experimental data. A complete tabulation of experimental and calculated values of conversion is given in (9).

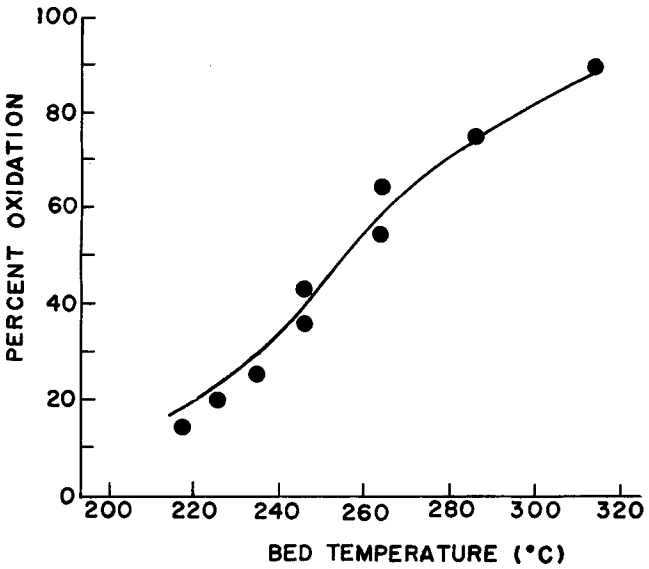

Fig. 9. Calculated and experimental data of ethylene oxidation on sample 3. Initial concentration of ethylene in ppm. • 500 at 220 liters/hr. Line: calculated data. Points: experimental data.

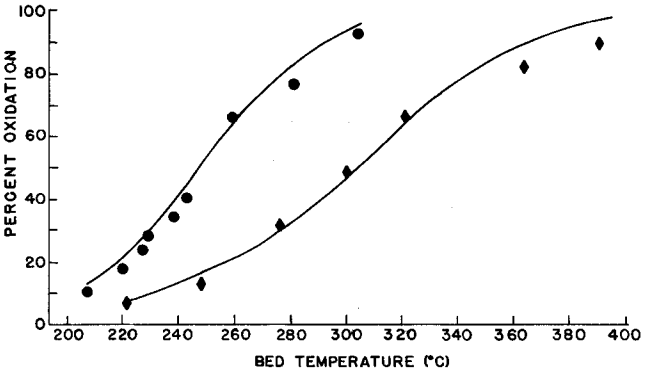

Fig. 10. Calculated and experimental data of ethylene oxidation on sample 4. Initial concentration of ethylene in ppm. • 500 at 120 liters/hr., ◇ 1,500 at 220 liters/hr. Lines: calculated data. Points: experimental data.

Calculated effectiveness factors were as low as 0.02 at high temperatures and low concentrations (that is, near the exit of the bed). Thus both experimental and calculated results show that pore diffusion plays an important role in the catalytic oxidation of hydrocarbons over copper oxide-alumina catalysts.

The effects of resistances to the transfer of heat and mass from the bulk gas stream to the external surface of the catalyst were evaluated by the calculation procedure. The maximum effects that were noted were a temperature rise of 5°K. (654°K. in the bulk stream; 659°K. at the external surface of the catalyst) and a drop in partial pressure amounting to 12% of the reactant partial pressure in the bulk gas phase. The net effect of these interphase resistances is to raise the reaction rate since the enhancement of the reaction rate due to the temperature rise more than compensates for the decrease in rate caused by the lower reactant partial pressure. It is interesting to note that although pore diffusion resistance plays a significant role in determining the overall rate, the interphase resistances are not so important. This is readily explained by the fact that pore diffusion depends on the specific rate constant while bulk transport effects depend on the value of the reaction rate. Thus, one would expect this situation in any system where the rate constant is high but the reactant concentration (and consequently the reaction rate) is low.

CONCLUSIONS

Pore diffusion effects were shown to be important in copper oxide-alumina catalysts used for the complete oxidation of hydrocarbons present in low concentrations. Presumably this would be important in any other reaction on these catalysts with a comparable reaction rate. A method has been developed to calculate the extent of reaction rate for reactions on these catalysts over a range of pellet sizes and temperatures. Satisfactory agreement between experimental and calculated results were obtained.

ACKNOWLEDGMENT

This investigation was supported by funds from the University of California Air Pollution Research program. L. S. Caretto acknowledges a Nat. Aeronaut. Space Admin. predoctoral traineeship held during the course of this work. Computer time was furnished by the University of Cailfornia at Los Angeles Computing Facility.

NOTATION

A = prefactor in Arrhenius equation, moles/g. cata-

lyst-sec.-atm.^{n}

a = radius of cylindrical pellets, cm.
C = concentration, moles/ml.
D = gas phase diffusion coefficient, sq.cm./sec.
D_e = effective diffusivity in catalyst pellet, sq.cm./sec.
D_k = Knudsen diffusion coefficient, sq.cm./sec.
D_{ab} = ordinary diffusion coefficient, sq.cm./sec.
E = Arrhenius activation energy, cal./mole
F = feed rate of reactant, moles/sec.
ΔH_R = heat of reaction, cal.
J_o = zeroth-order Bessel function of first kind
j_m = roots of equation $J_o(j_m) = 0$
k_v = rate constant, moles/sec.-ml. catalyst-(moles/ml.)^n
$\bar{k}_v$ = rate constant averaged over temperature profile in catalyst pellet
k_p = rate constant, moles/sec.-g. catalyst-atm.^{n}
l = height of cylindrical pellets, cm.
L = characteristic length of flat plate, cm.
m, n = dummy indices
n = reaction order
P = partial pressure of reactant, atm.
r = reaction rate, moles/sec.-g. catalyst
r_{avg} = average r over increment of catalyst bed
r_v = reaction rate, moles/sec.-ml. catalyst
$\bar{r}_v$ = average r_v for a catalyst pellet
R = gas constant
T = temperature, °K.
w = weight of catalyst, g.
x = conversion
z = variable length in direction of diffusion

Greek Letters

β = defined in Equation (9)
γ = defined in Equation (10)
Δ = finite difference
ϵ = pellet porosity
η = effectiveness factor
κ_e = effective thermal conductivity of catalyt
λ = $\sqrt{k_v/D_e}$
λ_n = defined in Equation (3)
ρ = radius of spherical pellet

Subscript

x = value of quantity at external surface of catalyst pellet

LITERATURE CITED

1. Accomazzo, M. A., Ph.D. dissertation, Univ. California, Los Angeles (June, 1963).
2. Anderson, J., *Chem. Eng. Sci.*, **18**, 147 (1963).
3. Aris, R., *ibid.*, **6**, 262 (1957).
4. ———, *Ind. Eng. Chem. Fundamentals*, **4**, 227 (1965).
5. ———, "Introduction to the Analysis of Chemical Reactors," Chap. 6, Prentice-Hall, Englewood Cliffs, N. J. (1965).
6. Bischoff, K., *AIChE J.*, **11**, 351 (1965).
7. Bosanquet, C., British T. A. Report, *BR 507* (1944) see (*16*).
8. Carberry, J., *AIChE J.*, **7**, 350 (1961).
9. Caretto, L. S., Ph.D. dissertation, Univ. California, Los Angeles (Sept., 1965).
10. ———, and Ken Nobe, *Ind. Eng. Chem. Process Design Develop.*, **5**, 207 (1966).
11. Damkohler, G., *Z. Phys. Chem.*, **A193**, 16 (1943).
12. Kittrell, J. R., and R. Mezaki, *Ind. Eng. Chem.*, **59**, 28 (1967).
13. Koutsoukos, E. P., and Ken Nobe, *Ind. Eng. Chem. Product. Res. Develop.*, **4**, 153 (1965).
14. Petersen, E. E., *Chem. Eng. Sci.*, **17**, 987 (1962).
15. Petersen, E. E., "Chemical Reaction Analysis," Chap. 4, Prentice-Hall, Englewood Cliffs, N. J. (1965).
16. Pollard, W. G., and R. D. Present, *Phys. Rev.*, **73**, 762 (1948).
17. Prater, C., *Chem. Eng. Sci.*, **8**, 284 (1958).
18. Satterfield, C. N., and T. K. Sherwood, "Role of Diffusion in Catalysis," Chap. 3, Addison-Wesley, Reading, Mass. (1963).
19. Sotoodehnia, A., unpublished results.
20. Weisz, P. B., and A. B. Schwartz, *J. Catalysis*, **1**, 399 (1962).
21. Yoshida, E., D. Ramaswami, O. A. Hougen, *AIChE J.*, **8**, 5 (1962).

Manuscript received September 27, 1967; revision received January 9, 1968; paper accepted January 15, 1968.

APPENDIX

EFFECTIVENESS FACTOR IN THE STRONG DIFFUSION REGION FOR AN n^{th} ORDER REACTION WITH SMALL HEAT EFFECTS

In the strong diffusion region the results for all geometries reduce to the flat plate solution if the characteristic length is taken as the ratio of pellet volume to geometric surface (3). The differential equation for the flat plate case is

$$D_e \frac{d^2C}{dz^2} = k_v C^n \qquad \text{(A1)}$$

In the strong diffusion region the boundary conditions are

$$C = 0 \text{ at } \frac{dC}{dz} = 0 \qquad C = C_x \text{ at } z = L \qquad \text{(A2)}$$

The effectiveness factor is given by

$$\eta = \frac{D_e \left(\frac{dC}{dz}\right)_{z=L}}{k_v(T_x) C_x{}^n L} \qquad \text{(A3)}$$

For small heat effects the rate constant can be expanded in Taylor series about the external surface temperature keeping only first-order terms

$$k_v = k_v(T_x)\left[1 + \frac{E}{RT^2{}_x}(T - T_x) + \cdots\cdots\right]$$

Equations (8), (9), and (10) can be used to express the temperature difference $T - T_x$ in terms of the concentration difference $C - C_x$. The resulting expression for k_v can then be substituted into Equation (A1) to give

$$\frac{d^2C}{dz^2} = \frac{k_v(T_x)}{D_e}\left[1 + \frac{\beta\gamma}{C_x}(C_x - C) \quad C^n\right]$$

This can be solved by defining $\omega = dC/dz$. Then d^2C/dz^2 becomes $\omega\, d\omega/dC$, and the equation can be readily integrated to give the concentration gradient (assuming $\beta\gamma$ and D_e constant)

$$\frac{dc}{dz} = \sqrt{2}\left[\frac{k_v(T_x)}{D_e}\right]^{1/2}\left[\frac{1 + \beta\gamma)}{n+1} C^{n+1} - \frac{\beta\gamma}{C_x}\frac{C^{n+2}}{n+2}\right]^{1/2}$$

When this is evaluated at z = L (C = C_x) and substituted into Equation (A3) the desired result for the effectiveness factor is obtained [using Equation (7) for λ_n]

$$\eta = \frac{1}{\lambda_n L}\left[1 + \frac{\beta\gamma}{n+2}\right]^{1/2} \qquad \text{(A4)}$$

For a sphere of radius ρ the ratio of volume to surface area is $\rho/3$. When this is substituted for L in the above equation, Equation (13) is obtained.

Petersen (*15*) has obtained expressions for the strong diffusion effectiveness factor for first and second-order reactions for any value of $\beta\gamma$. For small $\beta\gamma$ it can be shown that the results obtained from Equation (A4) are equivalent to Petersen's to first-order in $\beta\gamma$.